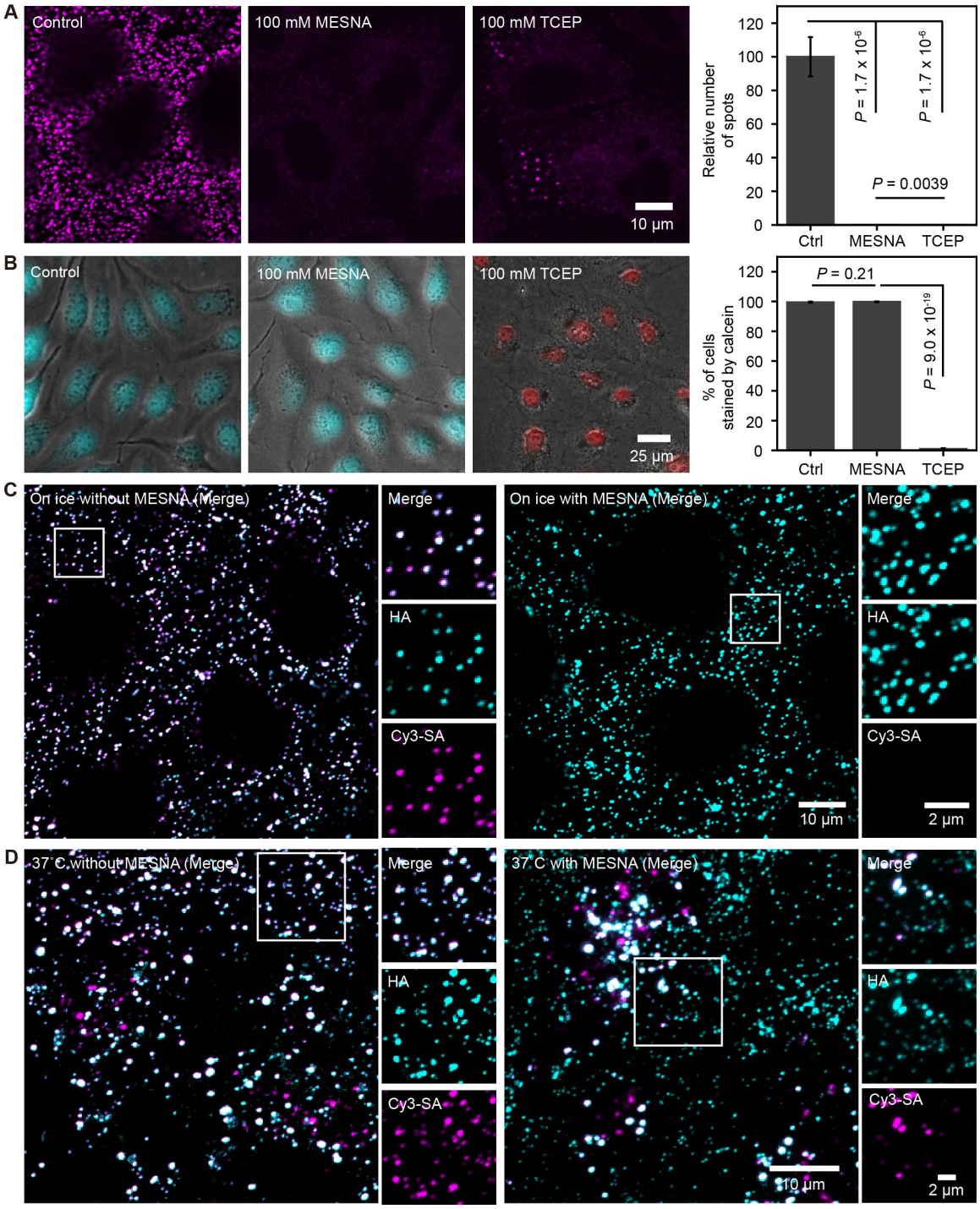

FIG S1 The use of MESNA and tris(2-carboxyethyl)phosphine (TCEP) in the IAV internalization assay (see also Fig. 1A).

(**A**) The removal of the biotin on the IAVs remaining on the cell surface is more complete using MESNA. Confocal fluorescence images of the biotin-conjugated IAV labeled with Cy3-SA (section through the middle of the cell; the same for **C**). The cells were

incubated with the biotin-conjugated IAV on ice, and then with 100 mM MESNA or 100 mM TCEP (or just buffer, Control) on ice, followed by paraformaldehyde fixation and further incubation with 100 nM Cy3-SA. The numbers of IAV spots, relative to the control sample, are shown in the graph on the right (Control, 81 cells in 12 images; MESNA, 76 cells in 12 images; TCEP, 78 cells in 12 images).

(**B**) TCEP, but not MESNA, permeabilized the PM, making TCEP unsuitable as a reagent to remove biotin only from the cell surface. Confocal images were overlayed with the phase-contrast images; typical among 8 images. Even after the MESNA treatment, calcein was incorporated in the cytoplasm and calcium ions were not leaked from the cytoplasm (cyan), and the membrane-impermeable propidium iodide did not enter the nucleus. Meanwhile, after the TCEP treatment, calcein leaked out of the cytoplasm and propidium iodide entered the nucleus to stain the DNA (red). For these experiments, after the cells were treated with MESNA or TCEP, they were further incubated with the mixture of membrane-impermeable propidium iodide, which fluoresces when it binds to DNA, and the acetoxymethyl (AM) ester of calcein (calcein-AM), which is membrane-permeable but becomes impermeable after the ester hydrolysis in the cytoplasm. The percentages of the cells containing calcein in the cytoplasm after the MESNA or TCEP treatment are shown in the graphs on the right (Control, 432 cells; MESNA, 498 cells; TCEP, 408 cells).

(**C, D**) Immunofluorescence staining with an anti-hemagglutinin (HA) monoclonal antibody, which binds to IAV both on the surface and in the cytoplasm. The cells were fixed and permeabilized before the Cy3-SA addition, confirmed that our cell-surface IAV detection method worked well (typical images). (**C**) Samples in which the IAV internalization was not induced, by keeping the specimen on ice (no incubation at 37˚C). The anti-HA spots (cyan) colocalized with the Cy3-SA spots (magenta) were 97.6 ± 0.68% and 0.012 ± 0.002% without and with the MESNA treatment (left and right), respectively, indicating that on the cell surface, the IAV detection by Cy3-SA was almost complete and the removal of biotin from IAV was almost complete, respectively (96 and 102 cells, respectively, in 25 images). The Cy3-SA spots colocalized with the anti-HA spots were 95.1 ± 0.98% and 100 ± 0% without and with the MESNA treatment, respectively, indicating the almost complete detection of IAV using the anti-HA

antibody. (**D**) Samples in which the IAV internalization was induced by incubation at 37˚C for 30 min. Without the MESNA treatment, virtually all of the anti-HA spots were colocalized with the Cy3-SA spots (74 cells in 10 images; left), whereas after treating the cells with MESNA (on ice to stop further internalization), the majorities of the anti-HA spots were not colocalized with the Cy3-SA spots, probably due to the removal of biotin from the IAV remaining on the cell surface (67 cells in 10 images; right). In both cases, several Cy3-SA spots that were not colocalized with the anti-HA spots appeared, mostly near the nucleus, and were probably located in lysosomes: the proteolytic digestion of IAV in lysosomes might have occurred, reducing the binding of the anti-HA antibody, but still allowing the binding of Cy3-SA.

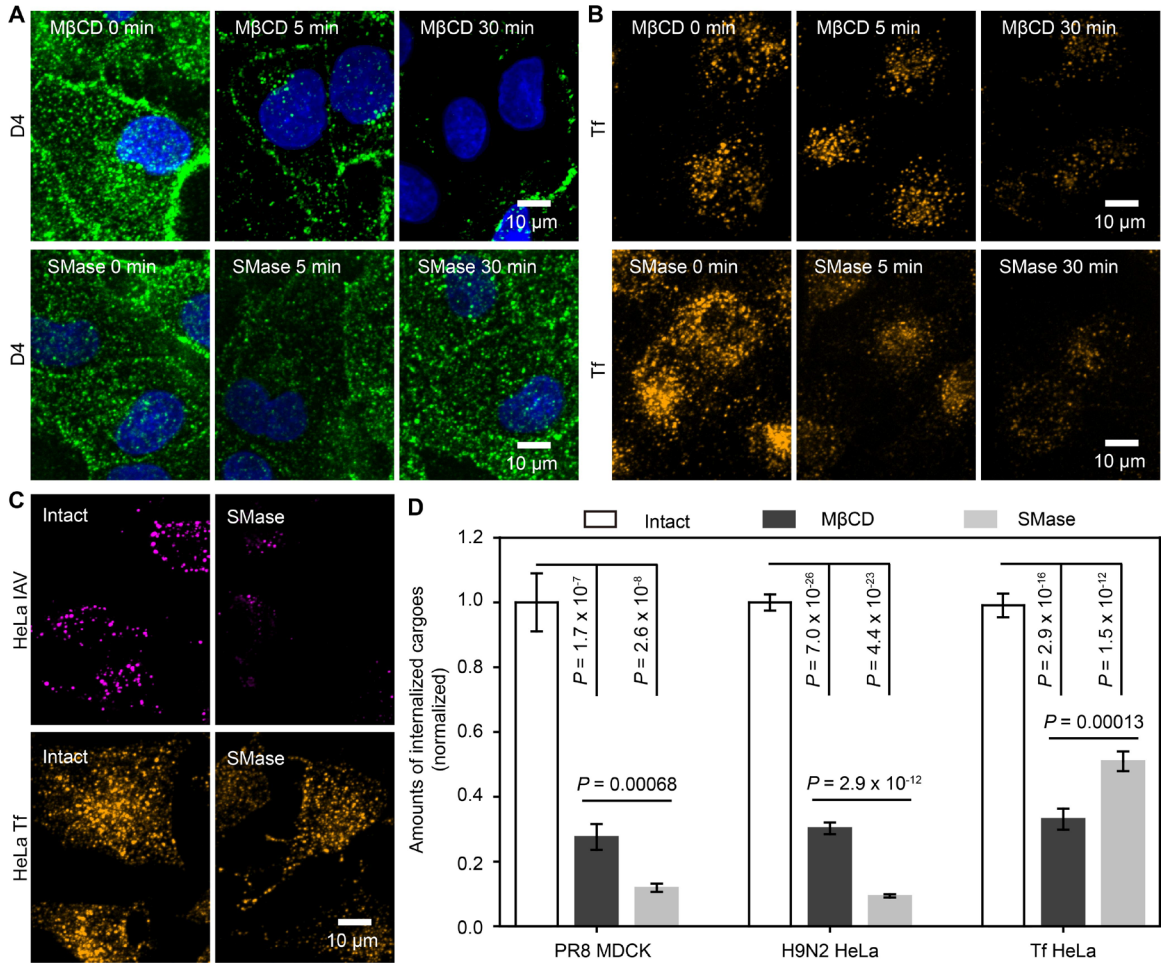

FIG S2 The effects of SMase and MβCD treatments (see Fig. 1B-E).

(**A**) Typical images (among 20 images) showing that the binding of mEGFP-D4, the probe for accessible cholesterol, to the PM outer leaflet decreased in time after the MβCD (**top**) and SMase (**bottom**) treatments.

(**B**) Typical images of internalized Tf in cells treated with MβCD and SMase (time courses). The numbers of images inspected: 25, 25 and 20 images from left to right (MβCD) and 20 images for all time points (SMase).

(**C**) HeLa cells exhibited decreases of IAV (**top**) and Tf (**bottom**) internalizations after the SMase treatment, similar to those found in MDCK cells, our standard cell line (**B and Fig. 1D-bottom**).

(**D**) The reductions of IAV and Tf internalization by the MβCD and SMase treatments using different IAV strain or cell lines are similar to those of the standard experimental system, with the H9N2 virus strain applied to MDCK cells (see **Fig. 1E** at 30 min). A

different IAV strain, PR8, applied to MDCK cells and the H9N2 IAV strain, our standard IAV strain, applied to a different host cell line HeLa. The internalization of Tf in a different cell line, HeLa, also exhibited similar reductions (see **Fig. 1E** at 30 min). For all conditions, >15 images each containing >100 cells were inspected.

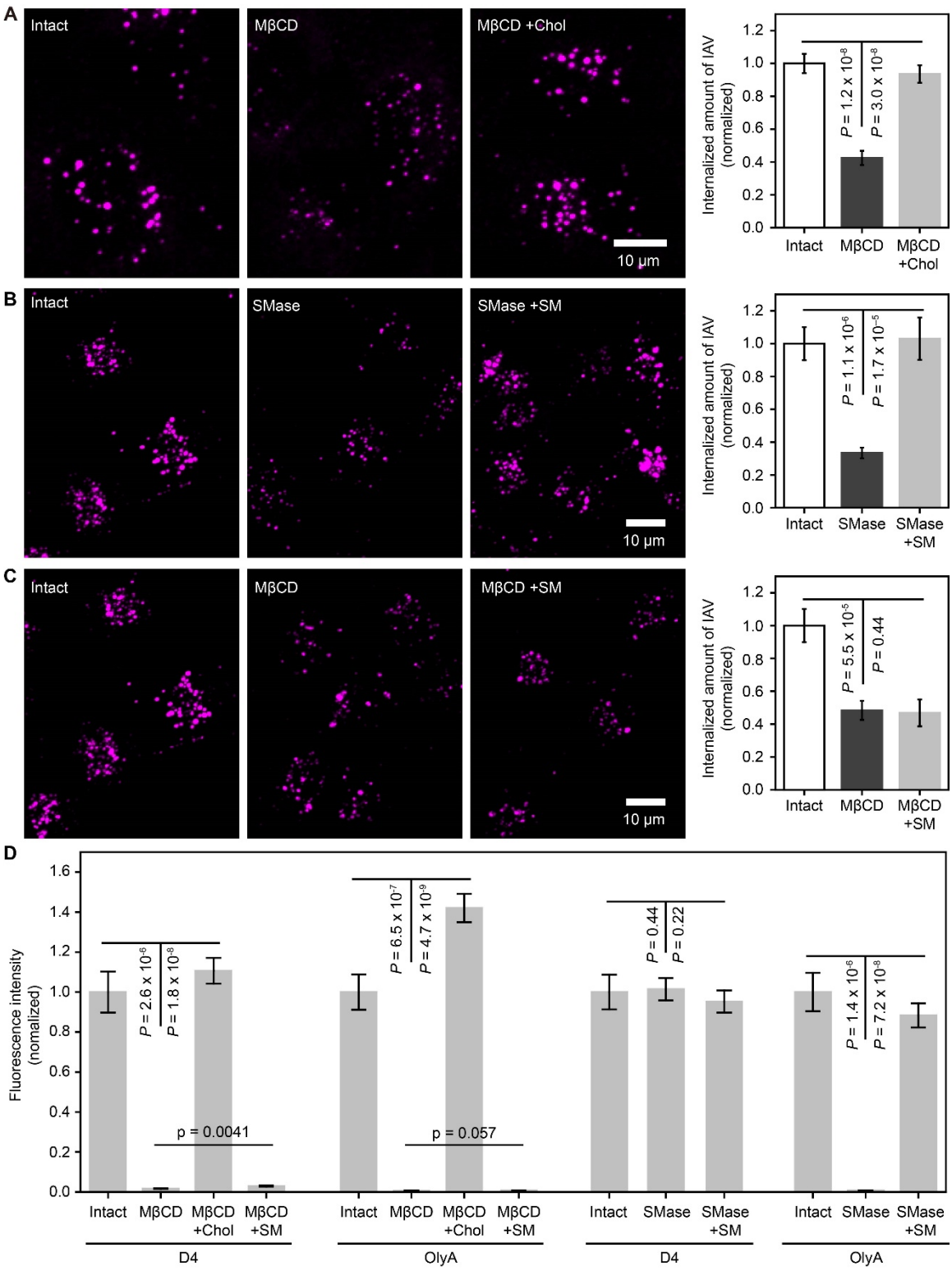

FIG S3 Replenishment of cholesterol (Chol) and sphingomyelin (SM) after the MβCD and SMase treatments, respectively, rescued the internalization of IAV.

(**A-C**) Typical images of internalized IAV in MDCK cells after 30 min IAV incubation at 37˚C, before and after the 30 min treatments with 10 mM MβCD (**A and C**) and 1.25 mU SMase (**B**), followed by replenishments with cholesterol (**A**; 10 mM cholesterol-saturated MβCD) and SM (**B and C**; 0.3 mM SM-BSA complex). The images are typical among 15 (**A**) and 20 (**B and C**) images. The quantified amounts of internalized IAV are shown on the right. (Intact) The control cells were treated with serum-free DMEM. The results in **C** show that the addition of SM could not rescue the effect of the MβCD treatment. (**D**) The replenishment of cholesterol and sphingomyelin after the MβCD and SMase treatments, respectively, restored the binding of D4 and OlyA. Neither D4-binding nor OlyA-binding was restored after the replenishment of sphingomyelin after the MβCD treatment.

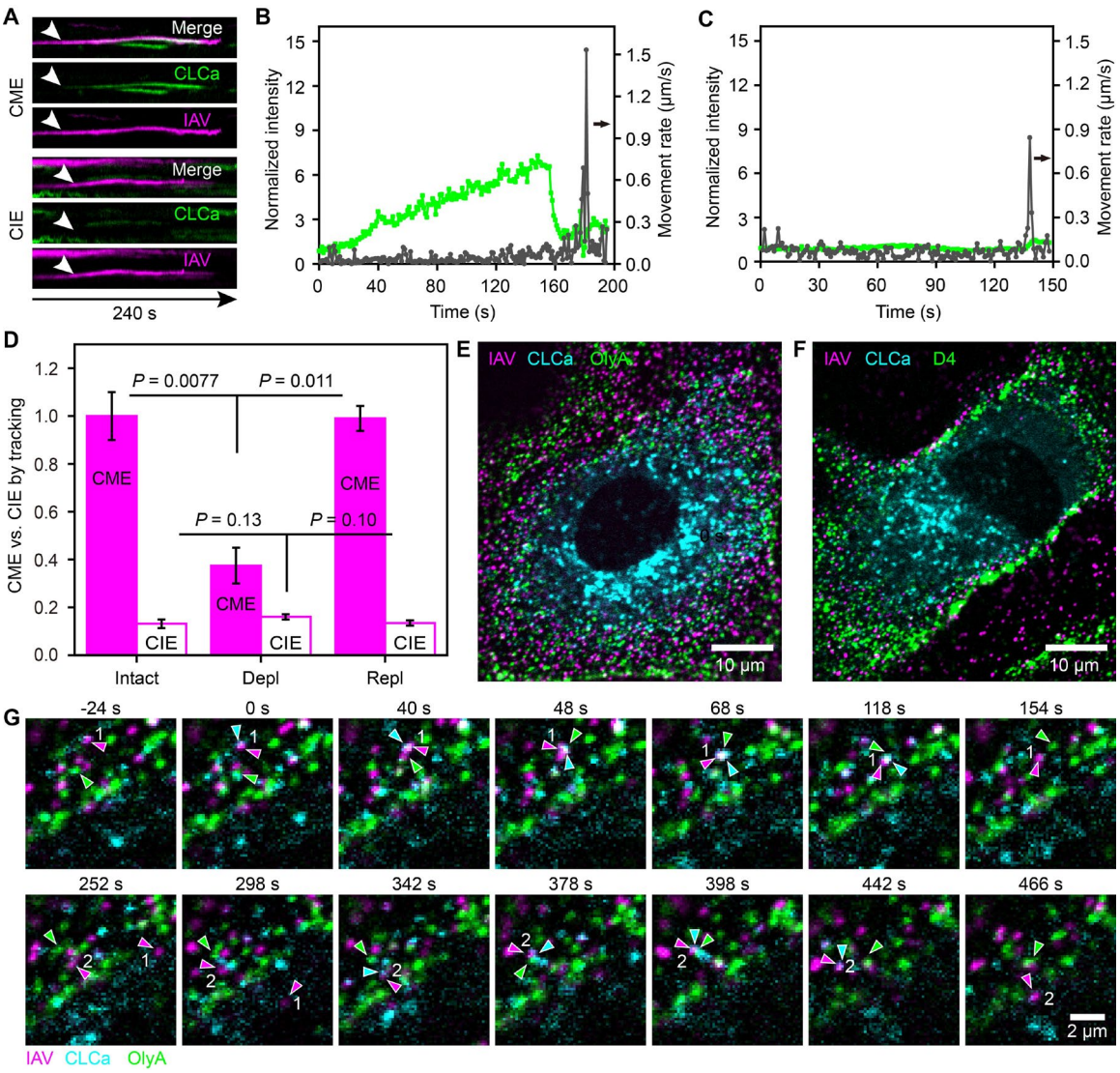

FIG S4 Discriminating the CME and CIE pathways for the IAV internalization using single-virus tracking.

(**A**) Typical kymographs of single IAV particles and single CCSs, showing that the CME and CIE of IAV could be distinguished by the formation of CCS spot at the IAV-binding site.

(**B, C**) The time courses of the fluorescence signal intensities of CLCa located in the square boxes containing the IAV particle shown in **Fig. 2A** (CME, **B**) and **Fig. 2B** (CIE, **C**), respectively. The black arrows represent the instantaneous rates of the IAV particle movement (see the y axis on the right).

(**D**) The effects of cholesterol depletion followed by cholesterol replenishment on the CME and CIE of IAV in HeLa cells. In intact HeLa cells, ~90% of internalized IAVs

entered via CME, whereas in MDCK cells, about 75% internalization was accomplished by CME. In HeLa cells, as in MDCK cells (**Fig. 2C**), the CME of IAV was decreased significantly after the MβCD treatment, whereas the CIE was unaffected. Intact, 96 IAVs in 40 cells; Depl (depletion of cholesterol by the MβCD treatment), 50 IAVs in 41 cells; Repl (replenishment of cholesterol), 87 IAVs in 36 cells.

(**E, F**) Typical tri-color confocal images (1 μm above the glass surface) showing IAV (magenta) bound to the surface of a live MDCK cell expressing mScarlet-I-CLCa (cyan), stained with the exogenously added OlyA-mEGFP (**E**, green; among 35 images) or mEGFP-D4 (**F**, green; among 30 images).

(**G**) Another typical tri-color confocal image sequence (see also **Fig. 2D**), showing two events that a SM-cholesterol domain became colocalized with an IAV-containing CCS. Images were obtained every 2 s. At time 0, the first event the CCS was formed at the place where the first internalized IAV bound.

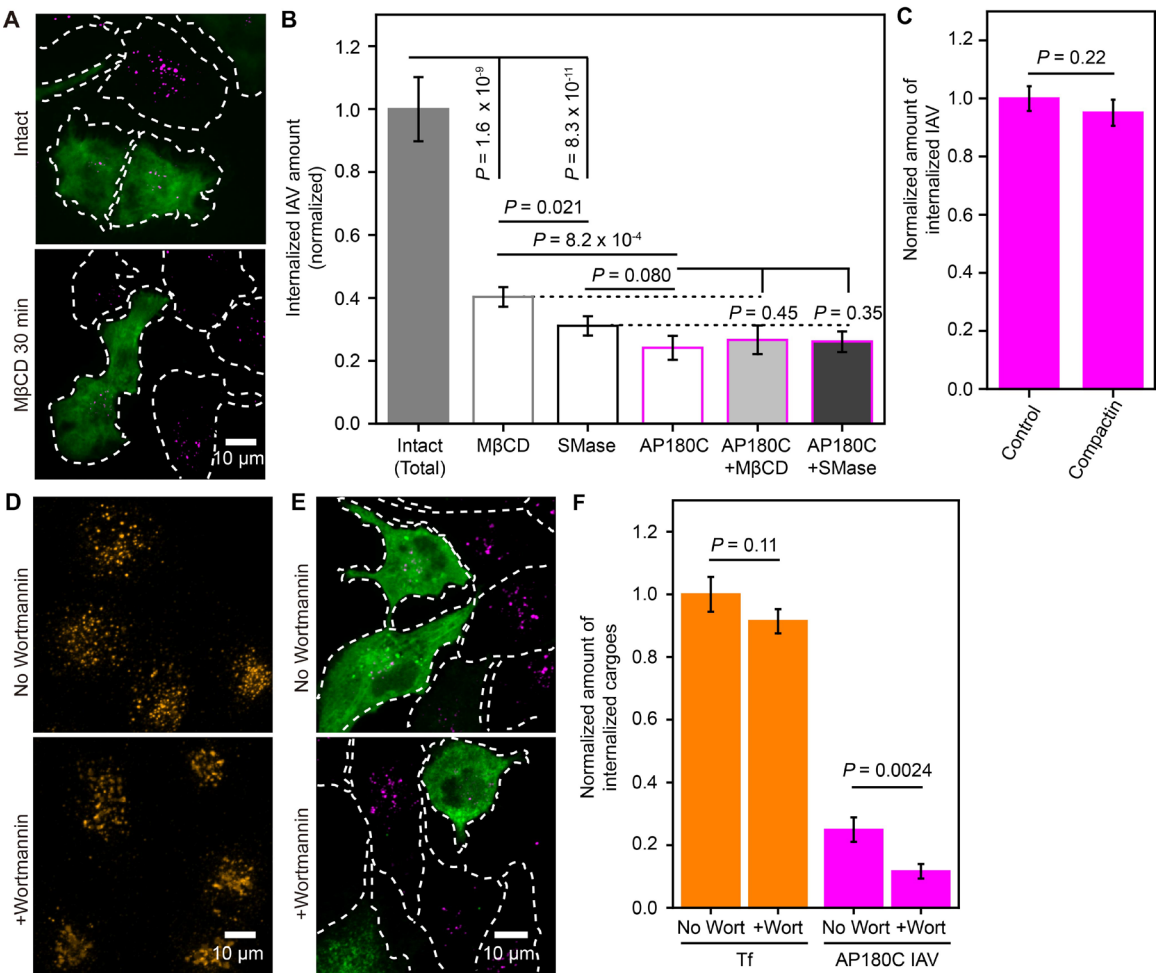

FIG S5 The CIE of IAV is not affected by the MβCD and SMase pretreatments (under conditions where CME is fully blocked by GFP-AP180C expression).

(**A**) Representative images showing the effect of the MβCD pretreatment for 30 min on the amounts of the internalized IAV (magenta) in cells with/without the expression of GFP-AP180C (green). No MβCD effect was apparent in the cells expressing GFP-AP180C, but the MβCD pretreatment greatly suppressed the IAV internalization in the cells that do not express GFP-AP180C (basic data for **Fig. S5B**).

(**B**) The amounts of internalized IAV and Tf (relative to the intact cells without any treatment) after treating the WT and AP180C-expressing cells with MβCD and SMase for 30 min. Neither the MβCD nor SMase treatment for 30 min changed the amounts of IAV internalized in AP180C-expressing cells (where all internalizations occur via CIE), indicating that the CIE of IAV is insensitive to cholesterol depletion (the fourth, fifth, and sixth bars from the left).

(**C**) IAV internalization was not reduced in accessible cholesterol-depleted cells cultured with 5% lipoprotein-deficient FBS, 50 μM sodium mevalonate, and 50 μM compactin for 48 h (Compactin). Control cells were cultured with 5% lipoprotein-deficient FBS, but without sodium mevalonateand and compactin for 48 h.

(**D**) Representative confocal microscope images (among 10 images) showing that wortmannin (a macropinocytosis inhibitor) preincubation does not affect the amount of internalized Tf (see **F**).

(**E**) Representative images showing that the expression of GFP-AP180C (green) reduced the internalized IAV (magenta; see **B** and **Fig. 2D**). Wortmannin significantly reduced the IAV internalization in AP180C expressing cells (i.e., the CIE of IAV; see **F**). Without wortmannin, 35 images; with wortmannin: 26 images.

(**F**) The CIE of IAV (AP180C expressing cells) is significantly blocked by preincubation with wortmannin (Wort) but the CME is not (as examined with Tf).

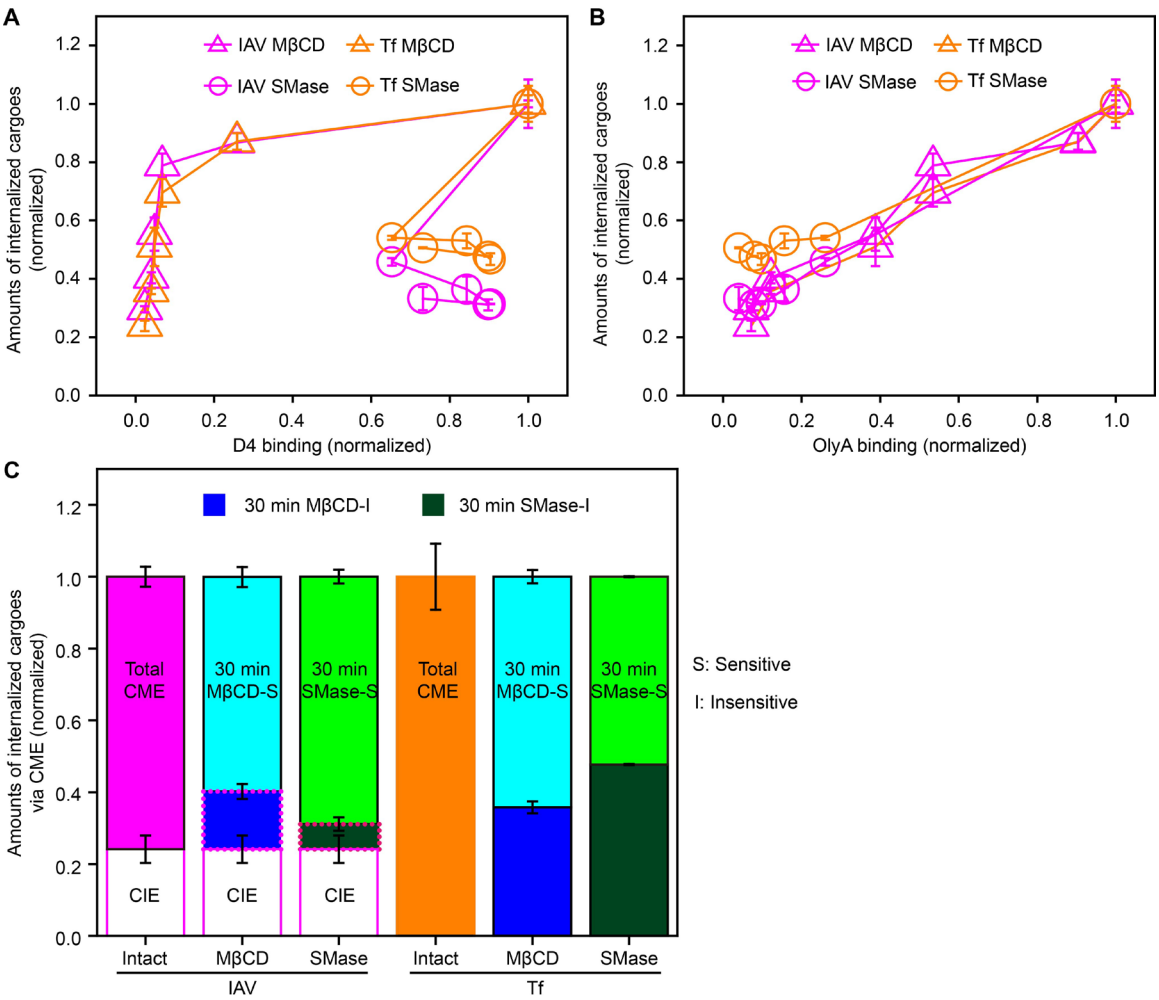

FIG S6 The CME of IAV depended on SM-sequestered cholesterol more than the CME of Tf (after treatments for 30 min and under high membrane tension).

(**A, B**) The total amounts of endocytosed IAV and Tf plotted as a function of the amounts of bound D4 (**A**) and OlyA (**B**), based on the data obtained after the MβCD and SMase treatments between 0 and 30 min (the plots for the data obtained after the treatments for 60 min are shown in **Fig. 4A, B**).

(**C**) The fractions of IAV and Tf internalized via different pathways in AP180C-expressing cells after the treatments with MβCD or SMase for 30 min. The fractions of CIE are taken from the results of AP180C-expressing cells in **Fig. 3D** (the sixth bar from the left; the difference is shown in the orange open bars; no CIE for Tf is assumed). The cyan and light-green parts of the bars represent the fractions of the internalized cargoes (IAV and Tf) sensitive to 30 min MβCD and SMase treatments, respectively (directly determined by experiments). The blue and dark-green parts of the bars represent the

fractions of the internalized cargoes (IAV and Tf) insensitive to 30 min MβCD and SMase treatments, respectively, which were calculated by subtracting the MβCD/SMase treatments-sensitive fraction from the fraction of CME, respectively.

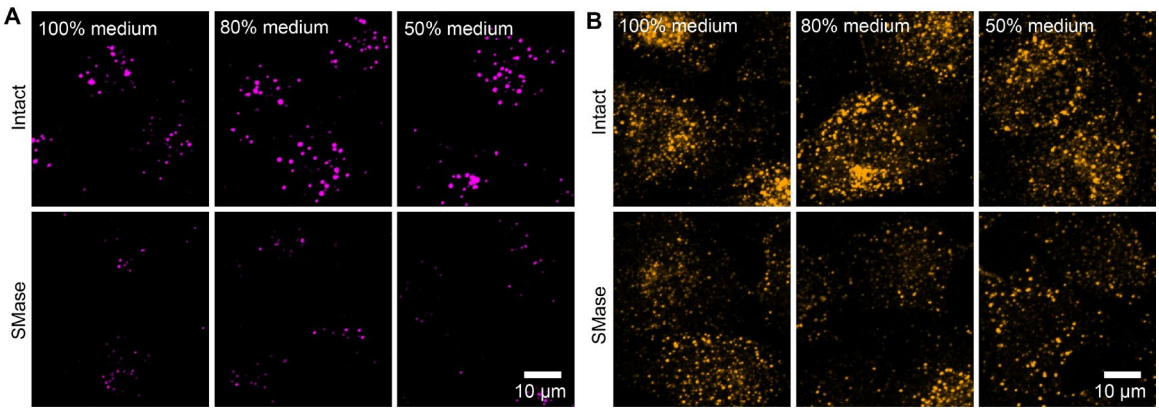

FIG S7 Typical images (among 20 images) showing that an increase in the membrane tension (with diluted media) enhanced the internalization of IAV (A), but not Tf (B), whereas the requirement of the SM-cholesterol complex for the internalizations of IAV and Tf persists even with higher membrane tension (see Fig. 4D).

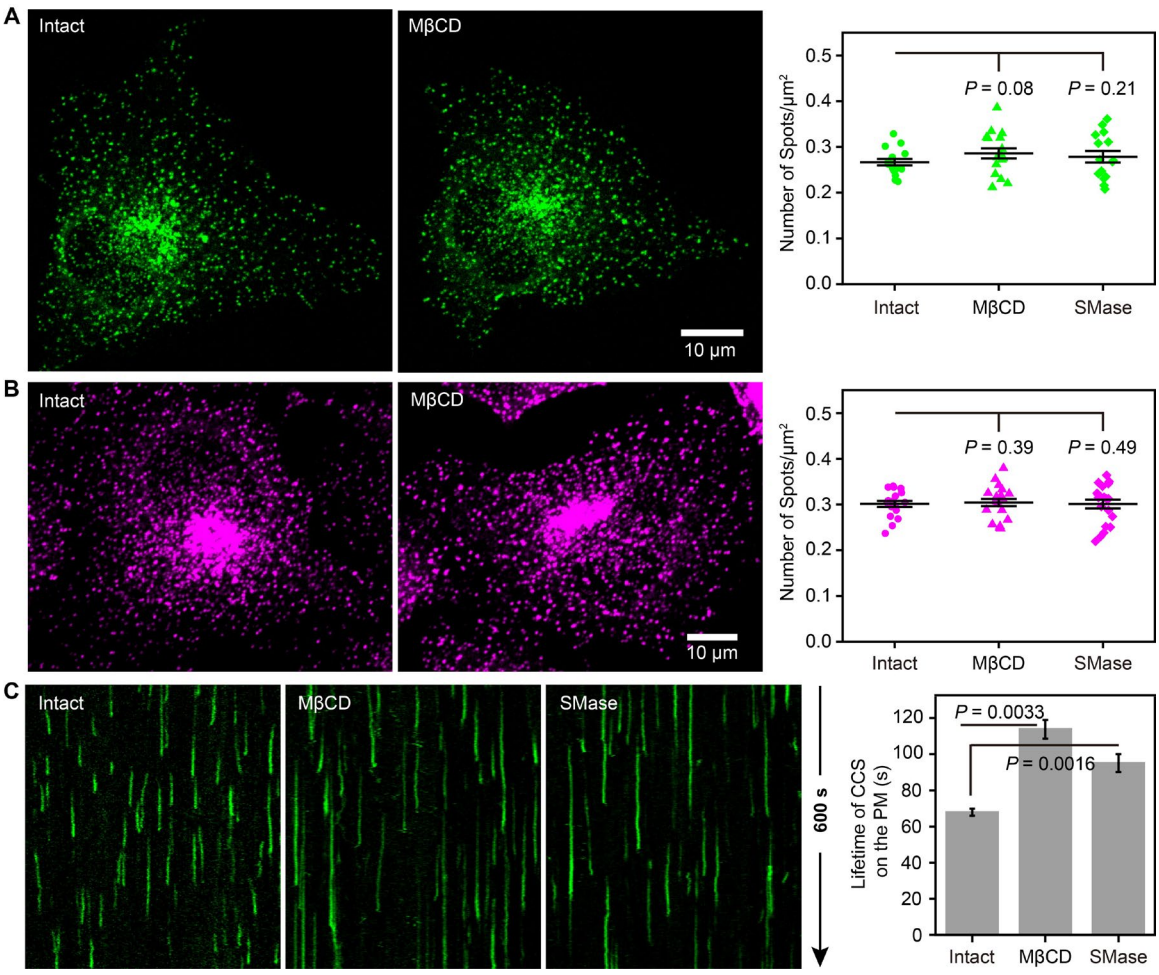

FIG S8 The MβCD and SMase treatments prolonged the CCS lifetime, without affecting the CCS densities on the PM.

(**A, B**) Typical maximum intensity projection images of the confocal 3D image slices are shown (see the graphs on the right for the n values). The MβCD and SMase treatments did not affect the density and distribution of CCSs on the PM. Confocal images of mEGFP-CLCa-transfected living cells (**A**) and immunolabeled fixed cells (**B**) before and after the MβCD treatment. The quantified densities of CCSs on the *basal* PM are shown on the right.

(**C**) Typical kymographs showing that the MβCD and SMase treatments prolonged the lifetime of CCSs on the basal PM. The quantifications of the CCS lifetimes on the *basal* PM are shown on the right (5,958 tracks in 3 cells; 2,129 tracks in 3 cells; and 4,218 tracks in 5 cells, respectively).

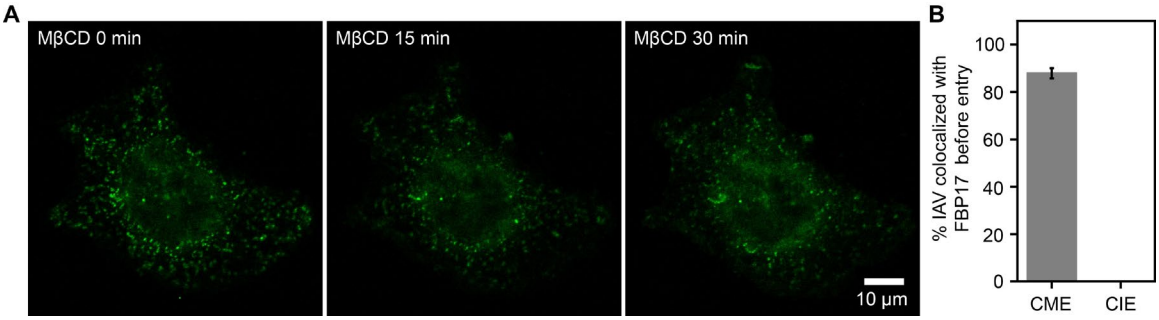

FIG S9 The MβCD incubation decreased the number density of FBP17 in the same cell (A) and FBP17 became colocalized with 88 ± 3% of IAV internalized by CME but did not colocalize with the IAV internalized by CIE (B, see Fig. 7A, 52 tracks in 20 cells).

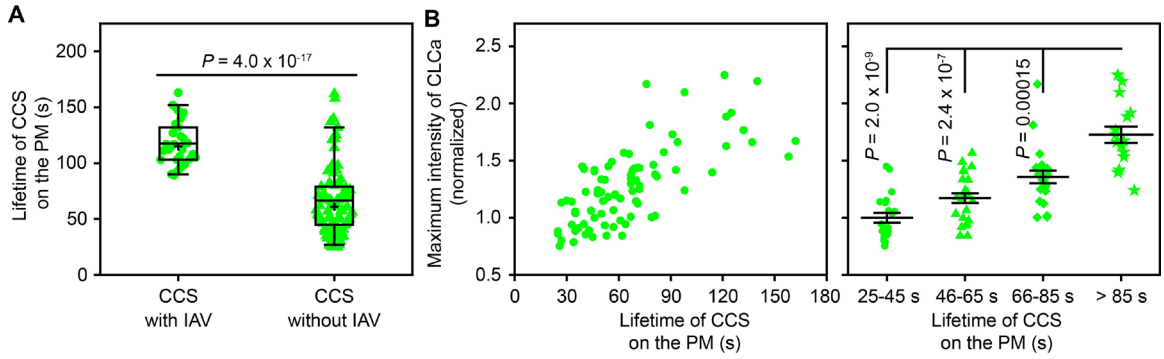

FIG S10 The CCSs colocalized with IAV exhibited much longer lifetimes on the PM.
(A) The residency lifetime of the CCSs bound by IAV before its internalization on the PM (CCS with IAV) was longer than that of the CCSs that were not bound by IAV (CCS without IAV). Horizontal bars, crosses, boxes, and whiskers indicate the median values, mean values, interquartile ranges (25–75%), and 10-90% ranges, respectively.
(B) The maximum fluorescence intensity of each CCS (mEGFP-CLCa) tended to become higher with a prolongation of its lifetime on the PM (CCS without IAV). The fluorescence intensity was normalized to the mean value of the maximum mEGFP-CLCa intensity of each CCS, with lifetimes between 25 and 45 s.

Table S1. Primers and RNAs sequences used in this study.

Name	Sequence
mEGFP-C1-F	tgtaccggtatggtgagcaagggcgag
mEGFP-C1-R	tgtagatctgagtccggacttgtacagctcgtccatgcc
mEGFP-N1-F	tgtaccggtatggtgagcaagggcgag
mEGFP-N1-R	ataagaatgcggccgcttacttgtacagctcgtccatgcc
SGSGx3-F	tctggtggcggatccgggggttcaggggggaggcagtgggggaagcggaggtgggtctggaggc
SGSGx3-R	gcctccagacccacctccgcttcccccactgcctccccctgaacccccggatccgccaccaga
CLCa-homo-F	tgtgaattctatggctgagctggatccg
CLCa-homo-R	tgtggtacctcagtgcaccagcgggg
CLCa-canis-F	tgtgaattctatggctgaactagatccgttcg
CLCa-canis-R	tgtggtacctcagtgcaccaaggggggc
mEGFP-pET-F	tgtaagcttatggtgagcaagggcgagg
mEGFP-pET-R	tgtctcgagttcgaaggtacccttgtacagctcgtccatgcc
mEGFP-pET-F’	tgtaagcttagcggaggtgggatggtgagcaagggcgagg
mEGFP-pET-R’	tgtctcgagttcgaaggtacctccgccaccagacttgtacag
D4H-S495D-F	gacggcaactaccaggacaagaccgcccac
D4H-S495D-R	gtgggcggtcttgtcctggtagttgccgtc
mEGFP-D4-F	tgtgaattatggtgagcaagggcgag
mEGFP-D4-R	tgtaagcttgttgtaggtgatgctgctgcc
OlyA-F	tgtgaattatggcgtacgcgcag
OlyA-R	tgtaagcttgttgccttttttcagggtatcaac
EndoA2-canis-F	tgtgaattcatgtcggtggcgggg
EndoA2-canis-R	tgtggtaccctgaggcaagggcaccag
EndoA2-homo-F	tgtgaattcatgtcggtggcgggg
EndoA2-homo-R	tgtggtaccctgcggcaggggcac
Epsin1-canis-F	tgtgaattcatgtcgacctcgtccctgc
Epsin1-canis-R	tgtggtaccgcctccacctcctgaccc
Epsin1-homo-F	tgtgaattcatgtcgacctcgtccttgagg
Epsin1-homo-R	tgtggtacctaggaggaagggattagtgttggg
FCHo2-canis-F	tgtgtcgacatgaaacatggacagatatcaac
FCHo2-canis-R	tgtgggcccctagataatctgccaggtatcgtcc
FCHo2-homo-F	tgtgaattctatggtcatggcgtatttcgtcg
FCHo2-homo-R	tgtgtcgactcaacaatccgccaggtatcgtc
FBP17-canis-F	tgtgaattctatgcttgaaaaggatcaatttgacaac

FBP17-canis-R	tgtggtacctcaaatataagtcttagcacctttggc
FBP17-homo-F	tgtgaattctatgagctggggcaccgag
FBP17-homo-R	tgtggtacctcaggaatctttggcatttttgtccaaacag
CIP4-canis-F	tgtaagcttatgcaggaagaccagacagc
CIP4-canis-R	tgtggtaccgttgagcgtgacacggagatag
CIP4-homo-F	tgtaagcttatggattggggcactgagc
CIP4-homo-R	tgtggtaccattgagcgtgactcggaggtag
Pacsin2-canis-F	tgtaagcttatgtctgtcgcttatgatgattccattg
Pacsin2-canis-R	tgtggtaccctggatcgcctcgacgtaattcg
Pacsin2-homo-F	tgtaagcttatgtctgtcacatatgatgattccgttg
Pacsin2-homo-R	tgtggtaccctggatcgcctccacataatttgc
SNX9-canis-F	tgtgaattctatggctcgggttatgtatgactttg
SNX9-canis-R	tgtggtaccctacatgactgggaagcggcc
SNX9-homo-F	tgtgaattctatggccaccaaggctcg
SNX9-homo-R	tgtggtaccctacatcactggaaagcggctgag
siFBP17	cca acc uga acg aaa uga aug auu a
siCtrl	uuc ucc gaa cgu guc acg utt